2 Electronic Structure in Semiconductor Nanocrystals: Optical Experiment[*]

David J. Norris

CONTENTS

---

[*] Portions of this chapter have been adapted (with permission) from D. J. Norris, PhD thesis, MIT, 1995.

2.1 INTRODUCTION

One of the primary motivations for studying nanometer-scale semiconductor crystallites, or nanocrystals, is to understand what happens when a semiconductor becomes small. This question has been studied not only for its fundamental importance, but also for its practical significance. As objects are rapidly shrinking in modern electronic and optoelectronic devices, we wish to understand their properties. To address this question, a variety of semiconductor nanocrystals have been investigated over the past two decades. Throughout these studies, one of the most important and versatile tools available to the experimentalist has been optical spectroscopy. In particular, it has allowed the description of how the electronic properties of these nanocrystals change with size. The purpose of this chapter is to review progress in this area.

The usefulness of spectroscopy stems from the inherent properties of bulk semiconductor crystals. Direct-gap semiconductors can absorb a photon when an electron is promoted directly from the valence band into the conduction band.[1] In this process, an electron–hole pair is created in the material, as depicted in Figure 2.1a. However, if the size of the semiconductor structure becomes comparable to or smaller than the natural length scale of the electron–hole pair, the carriers are confined by the boundaries of the material. This phenomenon, which is known as the *quantum size effect*, leads to atomic-like optical behavior in nanocrystals as the bulk bands become quantized (see Figure 2.1b). Since, at the atomic level, the material remains structurally identical to the bulk crystal, this behavior arises solely due to its finite size.
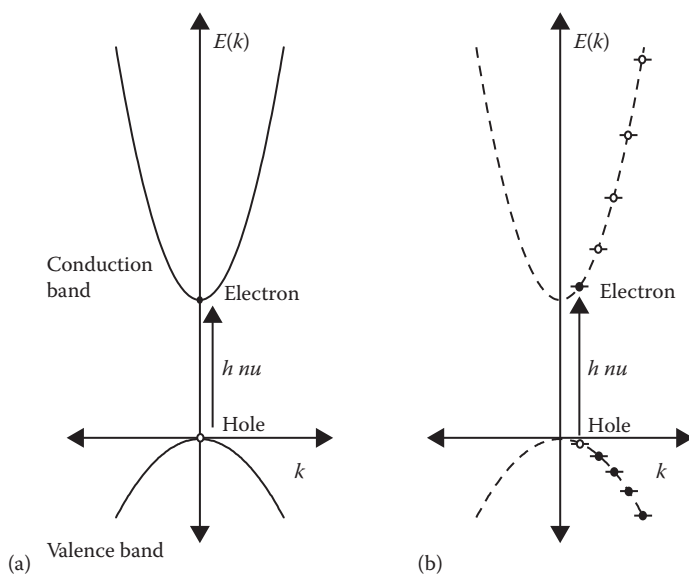

FIGURE 2.1 (a) Band diagram for a simple two band model for direct gap semiconductors. (b) Optical transitions in finite size semiconductor nanocrystals are discrete due to the quantization of the bulk bands.
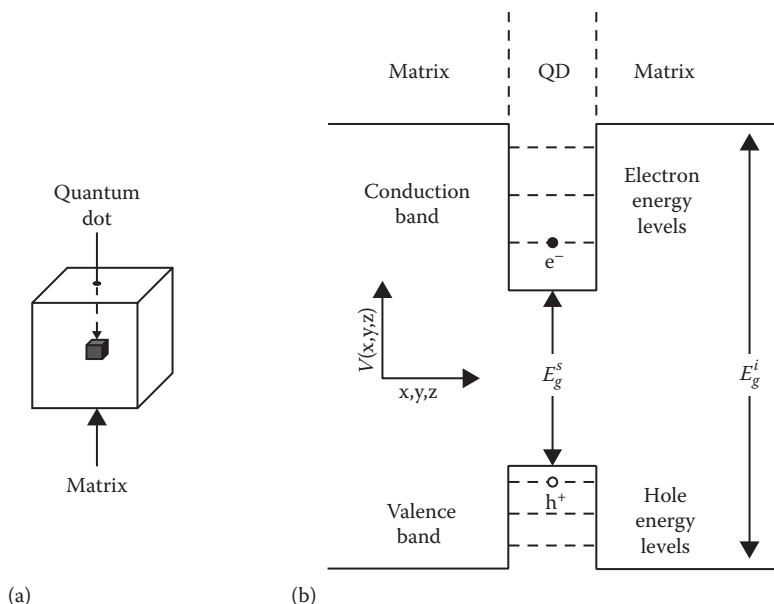
FIGURE 2.2 (a) Simple model of a nanocrystal (quantum dot) as a semiconductor inclusion embedded in an insulating matrix. (b) Potential well formed in any one dimension (x, y, or z) in the conduction and valence bands. The energy levels of the excited carriers (electrons and holes) become quantized due to the finite size of the semiconductor nanocrystal.

Therefore, by revealing this atomic-like behavior, simple optical data (e.g., absorption spectra) can give useful information about the nanometer size regime.

In many nanocrystal systems, this effect can be quite dramatic. Consequently, these materials, sometimes referred to as colloidal quantum dots, provide an easily realizable system for investigation of the nanometer size regime. Once this was realized, early research endeavored to explain the underlying phenomenon.[2–6] It was shown (see more later) that by modeling the quantum dot as a semiconductor inclusion embedded in an insulating matrix, as illustrated in Figure 2.2a, the basic physics could be understood. Photoexcited carriers reside in a three-dimensional potential well, as shown in Figure 2.2b. This causes the valence and conduction bands to be quantized into a ladder of hole and electron levels, respectively. Therefore, in contrast to the bulk absorption spectrum, which is a continuum above the band gap of the semiconductor (E_g^s),[1] spectra from semiconductor nanocrystals exhibit a series of discrete electronic transitions between these quantized levels. Accordingly, semiconductor nanocrystals are sometimes referred to as *artificial atoms*. Furthermore, since the energies of the electron and hole levels are quite sensitive to the amount of confinement, the optical spectra of nanocrystals are strongly dependent on the size of the crystallite.

To review recent progress in utilizing optical spectroscopy to understand this size dependence, we begin in Section 2.2 with a discussion of the basic theoretical concepts necessary to understand electronic structure in nanocrystals.

Then, experimental data from the prototypical direct gap semiconductor system, cadmium selenide (CdSe), is described in Section 2.3. As the first system to be successfully prepared with extremely high quality,[7] CdSe has been extensively studied. Indeed, it was the first system where the size dependence of the electronic structure was understood in detail.[8,9] Furthermore, this understanding led to the resolution of a long-standing mystery in semiconductor nanocrystals.[10,11] It was puzzling why these systems typically exhibit emission lifetimes that are two to three orders of magnitude longer than the bulk crystal. The origin of this phenomenon is explained in Section 2.3. Section 2.4 discusses recent work that moves beyond CdSe. In particular, InAs nanocrystals are described.[12] As a narrow-gap, III-V semiconductor, this system presents significant differences from CdSe. Studies of InAs have both confirmed and prompted further refinements in the theoretical model of nanocrystals.[13] Finally, Section 2.4 concludes by briefly outlining some of the remaining issues in the electronic structure of nanocrystals.

Unfortunately, this chapter does not provide a comprehensive review of nanocrystal spectroscopy. Therefore, the reader is encouraged to look at the other chapters of this book as well as the many excellent reviews and treatises that are now available on this topic.[14–21]

2.2 THEORETICAL FRAMEWORK

2.2.1 CONFINEMENT REGIMES

Earlier, we stated that the quantum size effect occurs when the size of the nanocrystal becomes comparable to or smaller than the *natural length scale* of the electron and hole. To be more precise, one can utilize the Bohr radius as a convenient length scale. In general, the Bohr radius of a particle is defined as

$$a_B = \varepsilon \frac{m}{m^*} a_o \qquad (2.1)$$

where:
   ε is the dielectric constant of the material,
   m^* is the mass of the particle,
   m is the rest mass of the electron, and
   a_o is the Bohr radius of the hydrogen atom[22]

(Note that throughout this chapter the term *particle* refers to an atomic particle, such as an electron or hole, *not* the nanocrystal.) For the nanocrystal, it is convenient to consider three different Bohr radii: one for the electron (a_e), one for the hole (a_h), and one for the electron–hole pair or exciton (a_{exc}). The latter is a hydrogenic-like bound state that forms in bulk crystals due to the Coulombic attraction between an electron and hole. Using Equation 2.1, each of these Bohr radii can be easily calculated. In the case of the exciton, the reduced mass of the electron–hole pair is used for *m**. With these values, three different limits can be considered.[2] First, when the nanocrystal radius, a, is much smaller than a_e, a_h, and a_{exc} (i.e., when $a < a_e$, a_h, a_{exc}), the electron and hole are each strongly confined by the nanocrystal boundary.

This is referred to as the *strong confinement regime*. Second, when a is larger than both a_e and a_h, but is smaller than a_{exc}, (i.e., when a_e, $a_h < a < a_{exc}$), only the center of mass motion of the exciton is confined. This limit is called the *weak confinement regime*. Finally, when a is between a_e and a_h (e.g., when $a_h < a < a_e$, a_{exc}), one particle (e.g., the electron) is strongly confined while the other (e.g., the hole) is not. This is referred to as the *intermediate confinement regime*.

Of course, the confinement regime, which is accessed in experiment, depends on the nanocrystal material and size. For example, since the exciton Bohr radius in InAs is 36 nm and nanocrystals are typically much smaller than this size, InAs nanocrystals are in the strong confinement regime. In contrast, CuCl has an exciton Bohr radius of 0.7 nm. Accordingly, CuCl nanocrystals are in the weak confinement regime. CdSe nanocrystals can be in either the strong confinement or the intermediate confinement regime, depending on the size of the nanocrystal, since a_{exc} is 6 nm.

2.2.2 THE *PARTICLE-IN-A-SPHERE* MODEL

Although the description of the different confinement regimes is useful, it does not provide a quantitative description of the size-dependent electronic properties. To move toward such a description, one can begin with a very simple model—the *particle-in-a-sphere* model.[2,6] In general, this model considers an arbitrary particle of mass m_o inside a spherical potential well of radius a:

$$V(r) = \begin{cases} 0 & r < a \\ \infty & r > a \end{cases} \tag{2.2}$$

Following Flügge,[23] the Schrödinger equation is solved yielding wavefunctions:

$$\Phi_{n,\ell,m}(r,\theta,\phi) = C \; \frac{j_\ell(k_{n,\ell}\, r)\; Y_\ell^m(\theta,\phi)}{r} \tag{2.3}$$

where:
C is a normalization constant,
$Y_\ell^m(\theta,\phi)$ is a spherical harmonic,
$j_\ell(k_{n,\ell}\, r)$ is the ℓth order spherical Bessel function, and

$$k_{n,\ell} = \alpha_{n,\ell}\big/a \tag{2.4}$$

where $\alpha_{n,\ell}$ is the nth zero of j_ℓ. The energy of the particle is given by

$$E_{n,\ell} = \frac{\hbar^2 k_{n,\ell}^2}{2\, m_o} = \frac{\hbar^2 \alpha_{n,\ell}^2}{2\, m_o\, a^2} \tag{2.5}$$

Owing to the symmetry of the problem, the eigenfunctions (Equation 2.3) are simple atomic-like orbitals that can be labeled by the quantum numbers n (1, 2, 3…), ℓ (s, p, d…), and m. The energies (Equation 2.5) are identical to the kinetic energy of the free particle, except that the wavevector, $k_{n,\ell}$, is quantized by the spherical boundary condition. Note also that the energy is proportional to $1/a^2$ and therefore is strongly dependent on the size of the sphere.

At first glance, this model may not seem useful for the nanocrystal problem. The particle above is confined to an empty sphere, while the nanocrystal is filled with semiconductor atoms. However, by a series of approximations, the nanocrystal problem can be reduced to the particle-in-a-sphere form (Equation 2.2). The photoexcited carriers (electrons and holes) may then be treated as particles inside a sphere of constant potential.

First, the bulk conduction and valence bands are approximated by simple isotropic bands within the *effective mass approximation*. According to Bloch's theorem, the electronic wavefunctions in a bulk crystal can be written as

$$\Psi_{nk}(\vec{r}) = u_{nk}(\vec{r}) \, \exp(i\,\vec{k}\cdot\vec{r}) \tag{2.6}$$

where u_{nk} is a function with the periodicity of the crystal lattice and the wavefunctions are labeled by the band index n and wavevector k. The energy of these wavefunctions is typically described in a *band diagram*, a plot of E versus k. Although band diagrams are in general quite complex and difficult to calculate, in the effective mass approximation the bands are assumed to have simple parabolic forms near extrema in the band diagram. For example, since CdSe is a direct gap semiconductor, both the valence band maximum and conduction band minimum occur at $k = 0$ (see Figure 2.1a). In the effective mass approximation, the energy of the conduction ($n = c$) and valence ($n = v$) bands are approximated as

$$
\begin{aligned}
E_k^c &= \frac{\hbar^2 k^2}{2\,m_{eff}^c} + E_g \\
E_k^v &= \frac{-\hbar^2 k^2}{2\,m_{eff}^v}
\end{aligned}
\tag{2.7}
$$

where E_g is the semiconductor band gap and the energies are relative to the top of the valence band. In this approximation, the carriers behave as free particles with an *effective mass*, $m_{eff}^{c,v}$. Graphically, the effective mass accounts for the curvature of the conduction and valence bands at $k = 0$. Physically, the effective mass attempts to incorporate the complicated periodic potential felt by the carrier in the lattice. This approximation allows the semiconductor atoms in the lattice to be completely ignored and the electron and hole to be treated as if they were free particles, but with a different mass.

However, to utilize the effective mass approximation in the nanocrystal problem, the crystallites must be treated as a bulk sample. In other words, we assume that the single particle (electron or hole) wavefunction can be written in terms of Bloch functions (Equation 2.6) and that the concept of an effective mass still has meaning in a small quantum dot. If this is reasonable, we can utilize the parabolic bands in Figure 2.1a to determine the electron levels in the nanocrystal, as shown in Figure 2.1b. This approximation, sometimes called the *envelope function approximation*,[24,25] is valid when the nanocrystal diameter is much larger than the lattice constant of the material. In this case, the single particle (*sp*) wavefunction can be written as a linear combination of Bloch functions:

$$\Psi_{sp}(\vec{r}) = \sum_k C_{nk} \, u_{nk}(\vec{r}) \, \exp(i\,\vec{k}\cdot\vec{r}) \tag{2.8}$$

where C_{nk} are expansion coefficients, which ensure that the sum satisfies the spherical boundary condition of the nanocrystal. If we further assume that the functions u_{nk} have a weak k dependence, then Equation 2.8 can be rewritten as

$$\Psi_{sp}(\vec{r}) = u_{n0}(\vec{r}) \sum_k C_{nk} \exp(i\,\vec{k}\cdot\vec{r}) = u_{n0}(\vec{r})\,f_{sp}(\vec{r}) \qquad (2.9)$$

where $f_{sp}(\vec{r})$ is the single particle *envelope function*. Since the periodic functions u_{n0} can be determined within the *tight-binding approximation* (or linear combination of atomic orbitals, LCAO, approximation) as a sum of atomic wavefunctions, φ_n,

$$u_{n0}(\vec{r}) \approx \sum_i C_{ni}\,\varphi_n(\vec{r}-\vec{r}_i) \qquad (2.10)$$

where the sum is over lattice sites and n represents the conduction band or valence band for the electron or hole, respectively; the nanocrystal problem is reduced to determining the envelope functions for the single particle wavefunctions, f_{sp}. Fortunately, this is exactly the problem that is addressed by the particle-in-a-sphere model. For spherically shaped nanocrystals with a potential barrier that can be approximated as infinitely high, the envelope functions of the carriers are given by the particle-in-a-sphere solutions (Equation 2.3). Therefore, each of the electron and hole levels depicted in Figure 2.2b can be described by an atomic-like orbital that is confined within the nanocrystal ($1S$, $1P$, $1D$, $2S$, etc.). The energy of these levels is described by Equation 2.5 with the free particle mass m_o replaced by $m_{eff}^{c,v}$.

So far, this treatment has completely ignored the Coulombic attraction between the electron and the hole, which leads to excitons in the bulk material. Of course, the Coulombic attraction still exists in the nanocrystal. However, how it is included depends on the confinement regime.[2] In the strong confinement regime, another approximation, the *strong confinement approximation*, is used to treat this term. According to Equation 2.5, the confinement energy of each carrier scales as $1/a^2$. The Coulomb interaction scales as $1/a$. In sufficiently small crystallites, the quadratic confinement term dominates. Thus, in the strong confinement regime, the electron and hole can be treated independently and each is described as a particle-in-a-sphere. The Coulomb term may then be added as a first-order energy correction, E_C. Therefore, using Equations 2.3, 2.5, and 2.9 the electron–hole pair (*ehp*) states in nanocrystals are written as

$$\Psi_{ehp}(\vec{r}_e,\vec{r}_h) = \Psi_e(\vec{r}_e)\,\Psi_h(\vec{r}_h) = u_c\,f_e(\vec{r}_e)\,u_v\,f_h(\vec{r}_h)$$

$$= C\left[u_c\,\frac{j_{L_e}(k_{n_e,L_e}r_e)\,Y_{L_e}^{m_e}}{r_e}\right]\left[u_v\,\frac{j_{L_h}(k_{n_h,L_h}r_h)\,Y_{L_h}^{m_h}}{r_h}\right] \qquad (2.11)$$

with energies

$$E_{ehp}(n_hL_hn_eL_e) = E_g + \frac{\hbar^2}{2a^2}\left\{\frac{\alpha^2_{n_h,L_h}}{m_{eff}^v}+\frac{\alpha^2_{n_e,L_e}}{m_{eff}^c}\right\} - E_c \qquad (2.12)$$

The states are labeled by the quantum numbers $n_hL_hn_eL_e$. For example, the lowest pair state is written as $1S_h1S_e$. For pair states with the electron in the $1S_e$ level, the

first-order Coulomb correction, E_c, is $1.8e^2/\varepsilon a$, where ε is the dielectric constant of the semiconductor.[4] Equations 2.11 and 2.12 are usually referred to as the particle-in-a-sphere solutions to the nanocrystal spectrum.

2.2.3 OPTICAL TRANSITION PROBABILITIES

The probability to make an optical transition from the ground state, $\left|0\right\rangle$, to a particular electron–hole pair state is given by the dipole matrix element

$$P = \left| \left\langle \Psi_{ehp} \left| \vec{e} \cdot \hat{p} \right| 0 \right\rangle \right|^2 \tag{2.13}$$

where $\vec{e}$ is the polarization vector of the light, and $\hat{p}$ is the momentum operator. In the strong confinement regime where the carriers are treated independently, Equation 2.13 is commonly rewritten in terms of the single particle states:

$$P = \left| \left\langle \Psi_e \left| \vec{e} \cdot \hat{p} \right| \Psi_h \right\rangle \right|^2 \tag{2.14}$$

Since the envelope functions are slowly varying in terms of $\vec{r}$, the operator $\hat{p}$ acts only on the unit cell portion (u_{nk}) of the wavefunction. Equation 2.14 is simplified to

$$P = \left| \left\langle u_c \left| \vec{e} \cdot \hat{p} \right| u_v \right\rangle \right|^2 \left| \left\langle f_e \left| f_h \right\rangle \right|^2 \tag{2.15}$$

In the particle-in-a-sphere model this yields

$$P = \left| \left\langle u_c \left| \vec{e} \cdot \hat{p} \right| u_v \right\rangle \right|^2 \delta_{n_e, n_h} \delta_{L_e, L_h} \tag{2.16}$$

due to the orthonormality of the envelope functions. Therefore, simple selection rules ($\Delta n = 0$ and $\Delta L = 0$) are obtained.

2.2.4 A MORE REALISTIC BAND STRUCTURE

In the preceding model, the bulk conduction and valence bands are approximated by simple parabolic bands (Figure 2.1). However, the real band structure of II-VI and III-V semiconductors is typically more complicated. For example, while the conduction band in CdSe is fairly well described within the effective mass approximation, the valence band is not. The valence band arises from Se *4p* atomic orbitals and is sixfold degenerate at $k = 0$, including spin. (In contrast, the conduction band arises from Cd *5s* orbitals and is only twofold degenerate at $k = 0$.) This sixfold degeneracy leads to valence band substructure that modifies the results of the particle-in-a-sphere model.[26]

To incorporate this structure in the most straightforward way, CdSe is often approximated as having an ideal diamond-like band structure, illustrated in Figure 2.3a. While the bands are still assumed to be parabolic, due to strong spin–orbit coupling ($\Delta = 0.42$ eV in CdSe[27]) the valence band degeneracy at $k = 0$ is split into $p_{3/2}$ and $p_{1/2}$ subbands, where the subscript refers to the angular momentum $J = l + s$ ($l = 1$, $s = 1/2$), where l is the orbital and s is the spin contribution to the angular momentum.
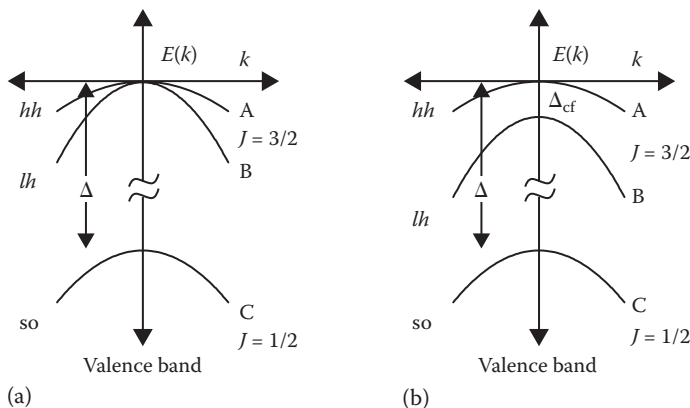
FIGURE 2.3 (a) Valence band structure at $k = 0$ for diamond-like semiconductors. Owing to spin–orbit coupling (Δ) the valence band is split into two bands ($J = 3/2$ and $J = 1/2$) at $k = 0$. Away from $k = 0$, the $J = 3/2$ band is further split into the $J_m = \pm 3/2$ heavy-hole (*hh* or A) and the $J_m = \pm 1/2$ light-hole (*lh* or B) subbands. The $J = 1/2$ band is referred to as the split-off (so or C) band. (b) Valence band structure for wurtzite CdSe near $k = 0$. Owing to the crystal field of the hexagonal lattice the A and B bands are split by Δ_{cf} (25 meV) at $k = 0$.

Away from $k = 0$, the $p_{3/2}$ band is further split into $J_m = \pm 3/2$ and $J_m = \pm 1/2$ sub-bands, where J_m is the projection of J. These three subbands are referred to as the heavy-hole (*hh*), light-hole (*lh*), and split-off-hole (*so*) subbands, as shown in Figure 2.3a. Alternatively, they are sometimes referred to as the *A*, *B*, and *C* subbands, respectively.

For many semiconductors, the diamond-like band structure is a good approxima-tion. In the particular case of CdSe, two additional complications arise. First, Figure 2.3a ignores the crystal field splitting that occurs in materials with a wurtzite (or hexagonal) lattice. This lattice, with its unique *c*-axis, has a crystal field that lifts the degeneracy of the *A* and *B* bands at $k = 0$, as shown in Figure 2.3b. This *A-B splitting* is small in bulk CdSe ($\Delta_{cf} = 25$ meV[27]) and is often neglected in quantum dot cal-culations. However, how this term can cause additional splittings in the nanocrystal optical transitions is discussed later.

The second complication is that, unlike the diamond structure, the hexagonal CdSe lattice does not have inversion symmetry. In detailed calculations, this lack of inversion symmetry leads to linear terms in *k*, which further split the *A* and *B* sub-bands in Figure 2.3b away from $k = 0$.[28] Since these linear terms are extremely small, they are generally neglected and are ignored in the following text.

2.2.5 THE $k \cdot p$ METHOD (PRONOUNCED K-DOT-P)

Owing to the complexity in the band structure, the particle-in-a-sphere model (Equation 2.11) is insufficient for accurate nanocrystal calculations. Instead, a better description of the bulk bands must be incorporated into the theory. While a vari-ety of computational methods could be used, this route does not provide analytical

expressions for the description of the bands. Thus, a more sophisticated effective mass approach, the $k \cdot p$ method, is typically used.[29] In this case, bulk bands are expanded analytically around a particular point in k-space, typically $k = 0$. Around this point the band energies and wavefunctions are then expressed in terms of the periodic functions u_{nk} and their energies E_{nk}.

General expressions for u_{nk} and E_{nk} can be derived by considering the Bloch functions in Equation 2.6. These functions are solutions of the Schrödinger equation for the single particle Hamiltonian:

$$H_0 = \frac{p^2}{2m_o} + V(x) \tag{2.17}$$

where $V(x)$ is the periodic potential of the crystal lattice. Using Equations 2.6 and 2.17, it is simple to show that the periodic functions, u_{nk}, satisfy the equation

$$\left[H_0 + \frac{1}{m_o}(k \cdot p) \right] u_{nk} = \lambda_{nk} u_{nk} \tag{2.18}$$

where

$$\lambda_{nk} = E_{nk} - \frac{-\,^2k^2}{2\,m_o} \tag{2.19}$$

Since u_{n0} and E_{n0} are assumed known, Equation 2.18 can be treated in perturbation theory around $k = 0$ with

$$H' = \frac{(k \cdot p)}{m_o} \tag{2.20}$$

Then by using nondegenerate perturbation theory to second order, one obtains the energies

$$E_{nk} = E_{n0} + \frac{\hbar^2 k^2}{2m_o} + \frac{1}{m_o^2} \sum_{m \neq n} \frac{\left| \vec{k} \cdot \vec{p}_{nm} \right|^2}{E_{n0} - E_{m0}} \tag{2.21}$$

and functions

$$u_{nk} = u_{n0} + \frac{1}{m_o} \sum_{m \neq n} u_{m0} \frac{\vec{k} \cdot \vec{p}_{mn}}{E_{n0} - E_{m0}} \tag{2.22}$$

with

$$\vec{p}_{nm} = \left\langle u_{n0} \left| \vec{p} \right| u_{m0} \right\rangle \tag{2.23}$$

The summations in Equations 2.21 and 2.22 are over all bands $m \neq n$. As one might expect the dispersion of band n is due to coupling with nearby bands. Also, note that inversion symmetry has been assumed. However, for hexagonal crystal lattices (i.e., wurtzite) like CdSe, the lack of inversion symmetry introduces linear terms in k into Equation 2.21. Since these terms are typically small, they are generally neglected.

With the $k \cdot p$ approach, analytical expressions can be obtained, which describe the bulk bands to second order in k. Although here the general method is outlined,

the approach must be slightly modified for CdSe. First, for the CdSe valence band, degenerate perturbation theory must be used. In this case, the valence band must be diagonalized before coupling with other bands can be considered. Second, we have neglected spin–orbit coupling terms. However, these terms are easily added as can be seen in Kittel.[29]

2.2.6 THE LUTTINGER HAMILTONIAN

For bulk diamond-like semiconductors, the sixfold degenerate valence band can be described by the Luttinger Hamiltonian.[30,31] This expression, a 6 by 6 matrix, is derived within the context of degenerate $k \cdot p$ perturbation theory.[32] The Hamiltonian is commonly simplified further using the *spherical approximation*.[33–35] Using this approach, only terms of spherical symmetry are considered. *Warping terms* of cubic symmetry are neglected and, if desired, treated as a perturbation. For nanocrystals, the Luttinger Hamiltonian (sometimes called the 6-band model) is the initial starting point for including the valence band degeneracies and obtaining the hole eigenstates and their energies. Note that since CdSe is wurtzite, as discussed earlier, use of the Luttinger Hamiltonian for CdSe quantum dots is an approximation. Most importantly, it does not include the crystal field splitting that is present in wurtzite lattices.

2.2.7 THE KANE MODEL

Although the Luttinger Hamiltonian is often suitable, particularly for describing the hole levels near k equal zero, for some situations it is necessary to go further. In particular, the Luttinger Hamiltonian does not include coupling between the valence and conduction bands, which can become significant, for example, in narrow gap semiconductors (see more details later). One approach would be to go to higher orders in $k \cdot p$ perturbation theory. However, because this can be quite cumbersome, Kane introduced an alternate procedure for bulk semiconductors, which is also widely used in nanoscale systems.[36–38] In the Kane model, a small subset of bands are treated exactly by explicit diagonalization of Equation 2.18 (or the equivalent expression with the spin–orbit interaction included). This subset usually contains the bands of interest, for example, the valence band and conduction band. Then the influence of outlying bands is included within the second-order $k \cdot p$ approach. Owing to the exact treatment of the important subset, the dispersion of each band is no longer strictly quadratic as in Equation 2.21. Therefore, the Kane model better describes band *nonparabolicities*. In particular, this approach is necessary for narrow gap semiconductors, where significant coupling between the valence and conduction bands occurs.

For semiconductor quantum dots, a Kane-like treatment was first discussed by Vahala and Sercel.[39,40] Recently, such a description has been used to successfully describe experimental data on narrow-bandgap InAs nanocrystals.[13] Furthermore, even wide-bandgap semiconductor nanocrystals, such as CdSe, may require a more sophisticated Kane treatment of the coupling of the valence and conduction bands.[41] These issues are discussed later.

2.3   CADMIUM SELENIDE NANOCRYSTALS

2.3.1   SAMPLES

Although the focus here is on nanocrystal spectroscopy, the importance of sample quality in obtaining useful optical information cannot be overemphasized. Indeed, a thorough understanding of the size dependence of the electronic structure in semiconductor quantum dots could not be achieved until sample preparation was well under control. Early spectroscopy (e.g., on II-VI semiconductor nanocrystals[5,42–51]) was constrained by distributions in the size and shape of the nanocrystals, which broaden all spectroscopic features, conceal optical transitions, and inhibit a complete investigation. Later, higher-quality samples became available in which many of the electronic states could be resolved.[52–55] However, the synthetic methods utilized to prepare these nanocrystals could not produce a complete series of such samples. Therefore, the optical studies were limited to one[52–54] or a few sizes.[55]

Fortunately, this situation has dramatically changed since the introduction of the synthetic method of Murray et al.[7] This procedure and subsequent variations[12,56–60] use a wet chemical (organometallic) synthesis to fabricate high-quality nanocrystals. From the original synthesis, highly crystalline, nearly monodisperse (<4% rms) CdSe nanocrystals can be obtained with well-passivated surfaces. Furthermore, by controlling the growth conditions, such samples can be easily obtained from ~0.8 to ~6 nm in mean radius. Thus, a complete size series can be investigated. For optical experiments, such samples are ideal. In particular, the intensity of *deep trap* emission, which dominates the luminescence behavior of dots prepared by many other methods, is very weak in these samples. Although the true origin of this emission is unknown, it is generally assumed to arise from surface defects, which are deep in the band gap. Instead of deep trap emission, the newer nanocrystals exhibit strong band-edge luminescence with quantum yields measured as high as 0.9 at 10 K. At room temperature the quantum yield is typically 10%. However, by encapsulating the CdSe nanocrystals in a higher band gap semiconductor, such as ZnS or CdS, the quantum yield can be further improved.[61–63] Emission efficiencies >0.5 at room temperature have been reported.

2.3.2   SPECTROSCOPIC METHODS

Samples obtained from these new synthetic procedures provided the first opportunity to study the size dependence of the electronic structure in detail. However, because even the best samples contain residual sample inhomogeneities, which can broaden spectral features and conceal transitions, several optical techniques have been used to reduce these effects and maximize the information obtained. These techniques include *transient differential absorption* (TDA) spectroscopy, *photoluminescence excitation* (PLE) spectroscopy, and *fluorescence line narrowing* (FLN) spectroscopy, which are described later. More recently, single molecule spectroscopy,[64] which can remove all inhomogeneities from the sample distribution, has been adapted to nanocrystals and many exciting results have been observed.[65] However, since *single quantum dot* spectroscopy is described elsewhere in this book and these methods

have mostly provided information about the emitting state (i.e., not the electronic level structure), it will not be emphasized here.

From a historical perspective, the most common technique to obtain absorption information has been TDA, also called pump-probe or hole-burning spectroscopy.[8,47,48,52–54,66–73] This technique measures the absorption change induced by a spectrally narrow pump beam. TDA effectively increases the resolution of the spectrum by optically exciting a narrow subset of the quantum dots. By comparing the spectrum with and without this optical excitation, information about the absorption of the subset is revealed with inhomogeneous broadening greatly reduced. Because the quantum dots within the subset are in an excited state, the TDA spectrum will reveal both the absence of ground-state absorption (a bleach) and excited-state absorptions (also called pump-induced absorptions). Unfortunately, when pump-induced absorption features overlap with the bleach features of interest, the analysis becomes complicated and the usefulness of the technique diminishes.

To avoid this problem, many groups have utilized another optical technique, PLE spectroscopy.[8,9,54,74–76] PLE is similar to TDA in that it selects a narrow subset of the sample distribution to obtain absorption information. However, in PLE experiments, one utilizes the emission of the nanocrystals. Thus, this technique is particularly suited to the efficient fluorescence observed in high-quality samples. PLE works by monitoring a spectrally narrow emission window within the inhomogenous emission feature while scanning the frequency of the excitation source. Because excited nanocrystals always relax to their first excited state before emission, the spectrum that is obtained reveals absorption information about the narrow subset of nanocrystals that emit.

An additional advantage of this technique is that emission information can be obtained during the same experiment. For example, FLN spectroscopy can be used to measure the emission spectrum from a subset of the sample distribution. In particular, by exciting the nanocrystals on the low energy side of the first absorption feature, only the largest dots in the distribution are excited.

Figure 2.4 demonstrates all of these techniques. In the top panel, absorption and emission results are shown for a sample of CdSe nanocrystals with a mean radius of 1.9 nm. On this scale, only the lowest two excited electron–hole pair states are observed in the absorption spectrum (solid line in Figure 2.4a). The emission spectrum (dashed line in Figure 2.4a) is obtained by exciting the sample well above its first transition so that emission occurs from the entire sample distribution. This inhomogeneously broadened emission feature is referred to as the *full luminescence* spectrum. If, instead, a subset of the sample distribution is excited, a significantly narrowed and structured FLN spectrum is revealed. For example, when the sample in Figure 2.4 is excited at the position of the downward arrow, a vibrational progression is clearly resolved (due to longitudinal optical [LO] phonons) in the emission spectrum. Similarly, by monitoring the emission at the position of the upward arrow, the PLE spectrum in Figure 2.4b reveals absorption features with higher resolution than in Figure 2.4a. Further, additional structure is observed within the lowest absorption feature. As discussed later, these features (labeled α and β) represent fine structure present in the lowest electron–hole pair state and have important implications for quantum dot emission. However, before discussing this fine structure, first the size dependence of the electron structure in CdSe nanocrystals is treated.

2.3.3 SIZE DEPENDENCE OF THE ELECTRONIC STRUCTURE

While the absorption and PLE spectra in Figure 2.4 show only the two lowest exciton features, high-quality samples reveal much more structure. For example, in Figure 2.5 PLE results for a 2.8 nm radius CdSe sample are shown along with its absorption and full luminescence spectra. These data cover a larger spectral range than Figure 2.4 and show more of the spectrum. To determine how the electronic structure evolves with quantum dot size, PLE data can be obtained for a large series of samples. Seven such spectra are shown in Figure 2.6. The nanocrystals are arranged (top to bottom) in order of increasing radius from ~1.5 to ~4.3 nm. Quantum confinement clearly shifts the transitions blue (>0.5 eV) with decreasing size. The quality of these quantum dots also allows as many as eight absorption features to be resolved in a single spectrum.

By extracting peak positions from PLE data, such as Figure 2.6, the quantum dot spectrum as a function of size is obtained. Figure 2.7 plots the result for a large data set from CdSe nanocrystals. Although nanocrystal radius (or diameter) is not used as the x-axis, Figure 2.7 still represents a size-dependent plot. The x-axis label, the energy of the first excited state, is a strongly size-dependent parameter. It is also much easier to measure accurately than nanocrystal size. For the y-axis, the energy
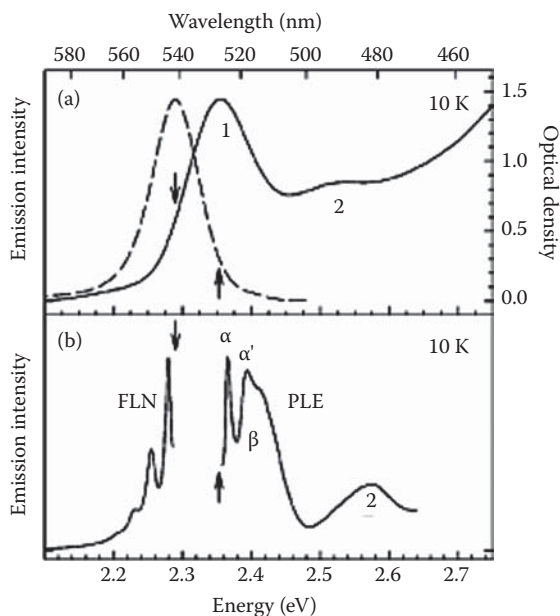

FIGURE 2.4 (a) Absorption (solid line) and full luminescence (dashed line) spectra for ~1.9 nm effective radius CdSe nanocrystals. (b) FLN and PLE spectra for the same sample. A LO-phonon progression is observed in FLN. Both narrow (α,α′) and broad (β) absorption features are resolved in PLE. The downward (upward) arrows denote the excitation (emission) position used for FLN (PLE). (Adapted from Norris, D. J., Al. L. Efros, M. Rosen, and M. G. Bawendi, *Phys. Rev. B,* 53, 16347, 1996.)
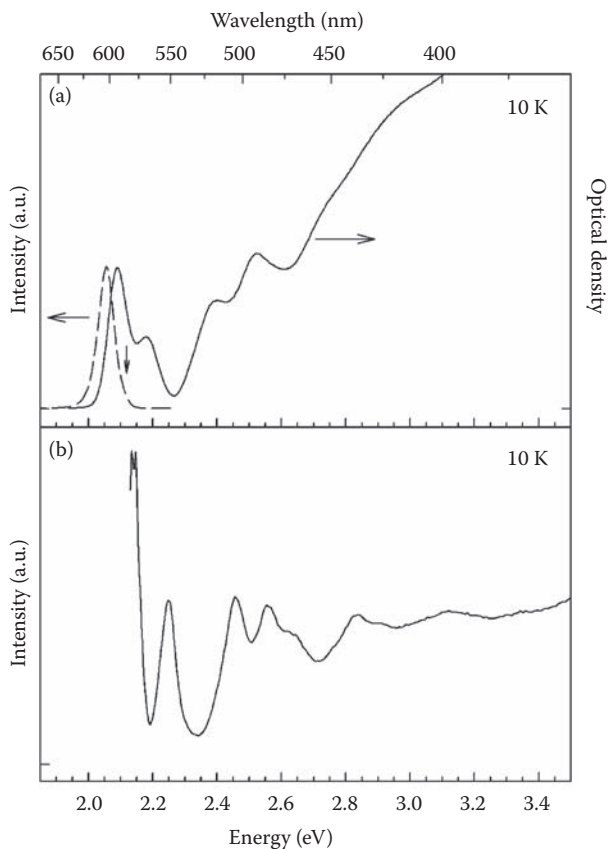
FIGURE 2.5 (a) Absorption (solid line) and full luminescence (dashed line) spectra for ~2.8 nm radius CdSe nanocrystals. In luminescence the sample was excited at 2.655 eV (467.0 nm). The downward arrow marks the emission position used in PLE. (b) PLE scan for the same sample. (Adapted from Norris, D. J. and M. G. Bawendi, *Phys. Rev. B,* 53, 16338, 1996.)

relative to the first excited state is used. This is chosen, in part, to concentrate on the excited states. However, it is also chosen to eliminate a difficulty in comparing the data with the theory, which is discussed later. This point aside, Figure 2.7 summarizes the size dependence of the first 10 transitions for CdSe quantum dots from ~1.2 to ~5.3 nm in radius. Since the exciton Bohr radius is 6 nm in CdSe, these data span the strong confinement regime in this material.

To understand this size dependence, one could begin with the simple particle-in-a-sphere model outlined earlier (Section 2.2.2). The complicated valence band structure, shown in Figure 2.3, could then be included by considering each subband (A, B, and C) as a simple parabolic band. In such a zero-th order picture, each bulk subband would lead to a ladder of particle-in-a-sphere states for the hole, as shown in Figure 2.8. Quantum dot transitions would occur between these hole states and
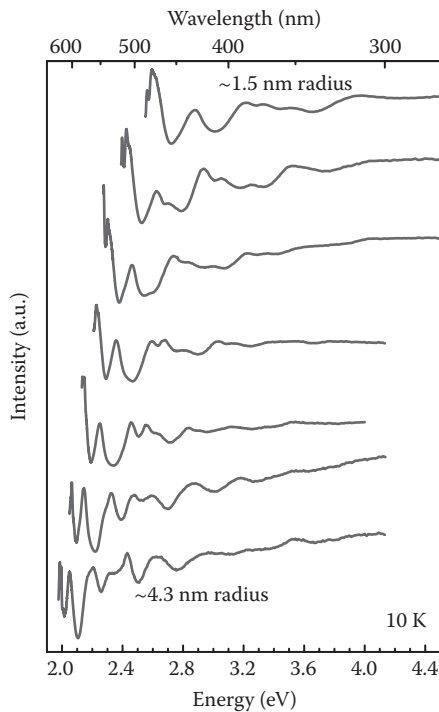
FIGURE 2.6 Normalized PLE scans for seven different size CdSe nanocrystal samples. Size increases from top to bottom and ranges from ~1.5 to ~4.3 nm in radius. (Adapted from Norris, D. J. and M. G. Bawendi, *Phys. Rev. B,* 53, 16338, 1996.)

the electron levels arising from the bulk conduction band. However, this simplistic approach fails to describe the experimental absorption structure. In particular, two avoided crossings are present in Figure 2.7 (between features [e] and [g] at ~2.0 eV and between features [e] and [c] above 2.2 eV) and these are not predicted by this particle-in-a-sphere model.

The problem lies in the assumption that each valence subband produces its own independent ladder of hole states. In reality, the hole states are mixed due to the underlying quantum mechanics. To help understand this effect, all of the relevant quantum numbers are summarized in Figure 2.9. The total angular momentum of either the electron or hole (F_e or F_h) has two contributions: (a) a "unit cell" contribution (J) due to the underlying atomic basis, which forms the bulk bands and (b) an envelope function contribution (L) due to the particle-in-a-sphere orbital. To apply the zero-th order picture (Figure 2.8), one must assume that the quantum numbers describing each valence subband (J_h) and each envelope function (L_h) are conserved. However, when the Luttinger Hamiltonian is combined with a spherical potential, mixing between the bulk valence bands occurs. This effect, which was first shown for bulk impurity centers,[33–35] also mixes quantum dot hole states.[26,39,40,55,77,78] Only parity and the total hole angular momentum (F_h) are good
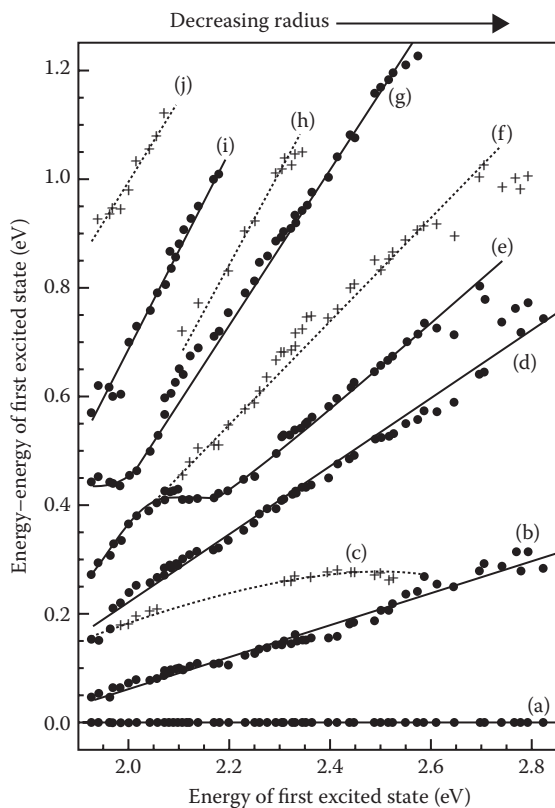
FIGURE 2.7 Size dependence of the electronic structure in CdSe nanocrystals. Peak positions are extracted from PLE data as in Figure 2.6. Strong (weak) transitions are denoted by circles (crosses). The solid (dashed) lines are visual guides for the strong (weak) transitions to clarify their size evolution. (Adapted from Norris, D. J. and M. G. Bawendi, *Phys. Rev. B,* 53, 16338, 1996.)

quantum numbers. Neither L_h nor J_h are conserved. Therefore, each quantum dot hole state is a mixture of the three valence subbands (*valence band mixing*) as well as particle-in-a-sphere envelope functions with angular momentum L_h and L_h+2 (*S-D mixing*). The three independent ladders of hole states, as shown in Figure 2.8, are coupled. The electron levels, which originate in the simple conduction band that is largely unaffected by the valence band complexities, can be assumed to be well described by the particle-in-a-sphere ladder. However, this assumption will be revisited later.

When the theory includes these effects, the size dependence observed in Figure 2.7 can be described. Using the approach of Efros et al.,[55,77] in which the energies of the hole states are determined by solving the Luttinger Hamiltonian and the electron levels are calculated within the Kane model, strong agreement with the data is obtained, as shown in Figures 2.10 and 2.11. Figure 2.10 compares the theory with the lowest
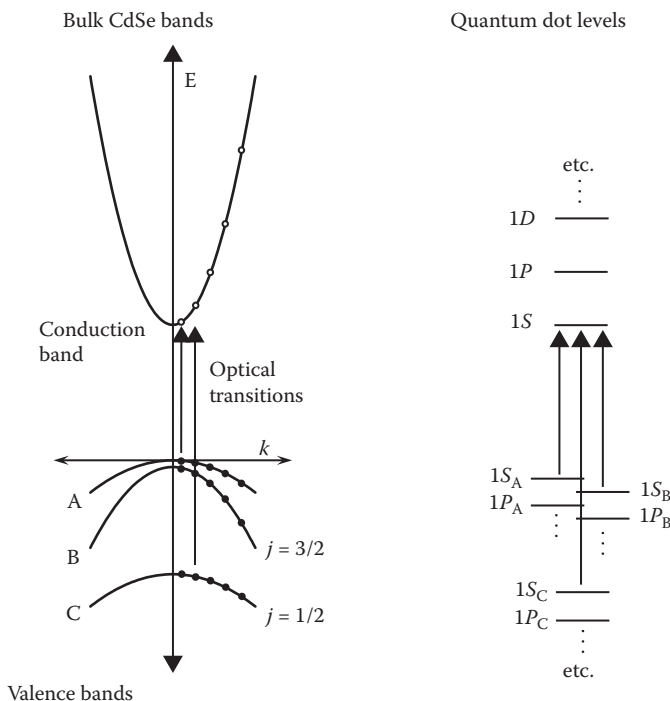
FIGURE 2.8 A simplistic model for describing the electronic structure in nanocrystals. Each valence band contributes a ladder of particle-in-a-sphere states for the hole. The optical transitions then occur between these hole states and the electron levels arising from the conduction band. This model fails to predict the observed structure due to mixing of the different hole ladders, as discussed in the text.

three transitions that exhibit simple size-dependent behavior (i.e., no avoided crossings). Figure 2.11 shows the avoided crossing regions. The transitions can be assigned and labeled by modified particle-in-a-sphere symbols, which account for the valence band mixing discussed earlier.[9]

Although the theory clearly predicts the observed avoided crossings, Figure 2.11 also demonstrates that the theory underestimates the repulsion in both avoided crossing regions, causing theoretical deviation in the predictions of the $1S_{1/2}1S_e$ and $2S_{1/2}1S_e$ transitions. This discrepancy could be due to the Coulomb mixing of the electron–hole pair states, which is ignored by the model (via the strong confinement approximation). If included, this term would further couple the $nS_{1/2}1S_e$ transitions such that these states interact more strongly. In addition, the Coulomb term would cause the $1S_{1/2}1S_e$ and $2S_{1/2}1S_e$ states to avoid one another through their individual repulsion from the strongly allowed $1P_{3/2}1P_e$.

Despite these discrepancies, however, this theoretical approach is clearly on the right track. Therefore, this model can be used to understand the physics behind the avoided crossings. As discussed earlier, in the zero-th order picture of Figure 2.8, each valence subband contributes a ladder of hole states. Owing to spin–orbit splitting
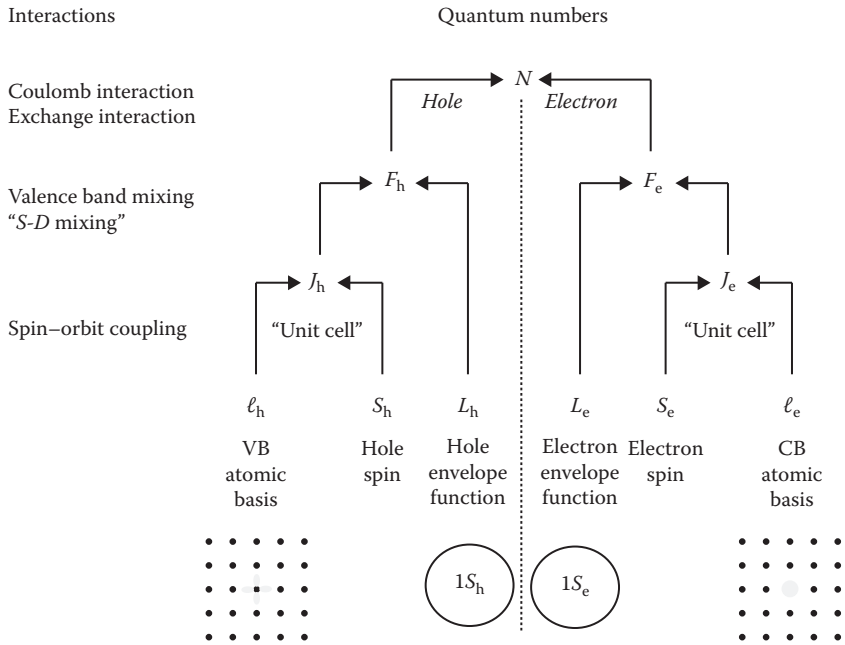
Interactions   Quantum numbers

Coulomb interaction
Exchange interaction

Valence band mixing
"S-D mixing"

Spin–orbit coupling

FIGURE 2.9 Summary of quantum numbers and important interactions in semiconductor nanocrystals. The total electron–hole pair angular momentum (N) has contributions due to both the electron (F_e) and hole (F_h). Each carrier's angular momentum (F) may then be further broken down into a unit cell component (J) due to the atomic basis (ℓ) and spin (S) of the particle and an envelope function component (L) due to the particle-in-a-sphere orbital.

the C-band ladder is offset 0.42 eV below the A- and B-band ladders. This leads to possible resonances between hole levels from the A and B bands with C band levels. Since the levels are spreading out with decreasing dot size, resonance conditions are satisfied only in certain special sizes. Figure 2.12 demonstrates the two resonances responsible for the observed avoided crossings. For simplicity, the A and B bands are treated together. In Figure 2.12a and b, the $2D$ ($1D$) level from the A and B bands is resonant with the $1S$ level from the C band. The size dependence of these levels is depicted in Figure 2.12c. Owing to both valence band mixing and S-D mixing, these resonant conditions lead to the observed avoided crossings. Although this description is based on the simple particle-in-a-sphere model of Figure 2.8, the explanation has been shown to be consistent with a more detailed analysis.[9]

2.3.4 BEYOND THE SPHERICAL APPROXIMATION

The success achieved earlier in describing the size dependence of the data was achieved within the *spherical approximation* (Section 2.2.6). In this case, the bands are assumed to be spherically isotropic (i.e., warping terms in Equation 2.21 are ignored). Furthermore, the CdSe nanocrystals are assumed to have a spherical shape and a cubic crystal lattice (i.e., zinc blende). With these assumptions, each
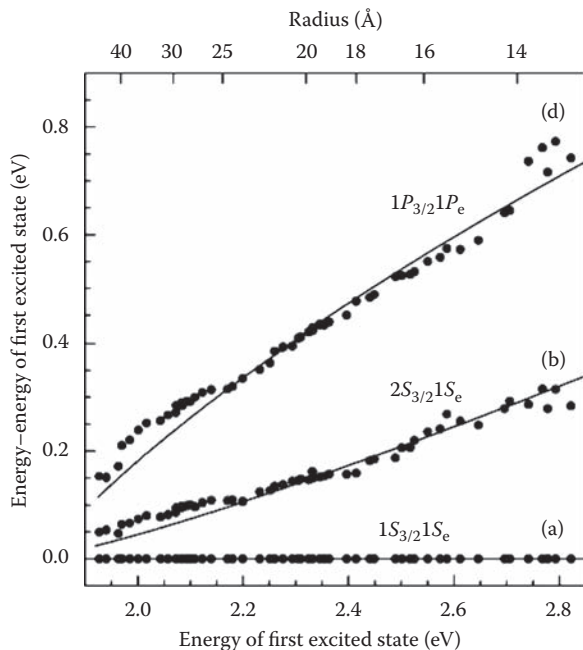
FIGURE 2.10 Theoretically predicted pair states (solid lines) assigned to features (a), (b), and (d) in Figure 2.7. The experimental data are shown for comparison (circles). (Adapted from Norris, D. J. and M. G. Bawendi, *Phys. Rev. B,* 53, 16338, 1996.)

of the electron–hole pair states is highly degenerate. For example, the first excited state ($1S_{3/2}1S_e$—which is referred to as the *band-edge exciton*) is eightfold degenerate. However, in reality, these degeneracies will be lifted by several second-order effects. First, as mentioned earlier, CdSe nanocrystals have a unixial crystal lattice (wurtzite), which leads to a splitting of the valence subbands (Figure 2.3b).[79] Second, electron microscopy experiments show that CdSe nanocrystals are not spherical, but rather slightly prolate.[7] This shape anisotropy will split the electron–hole pair states.[80] Finally, the electron–hole exchange interaction, which is negligible in bulk CdSe, can lead to level splittings in nanocrystals due to enhanced overlap between the electron and hole.[81–84] Therefore, when all of these effects are considered, the initially eightfold degenerate band-edge exciton is split into five sublevels.[10]

This *exciton fine structure* is depicted in the energy-level diagram of Figure 2.13. To describe the structure, two limits are considered. On the left side of Figure 2.13, the effect of the anisotropy of the crystal lattice or the nonspherical shape of the crystallite dominates. This corresponds to the bulk limit where the exchange interaction between the electron and hole is negligible (0.15 meV).[85] The band-edge exciton is split into two fourfold degenerate states, analogous to the bulk A-B splitting (see Figure 2.3b). The splitting occurs due to the reduction from spherical to uniaxial symmetry. However, since the exchange interaction is proportional to the
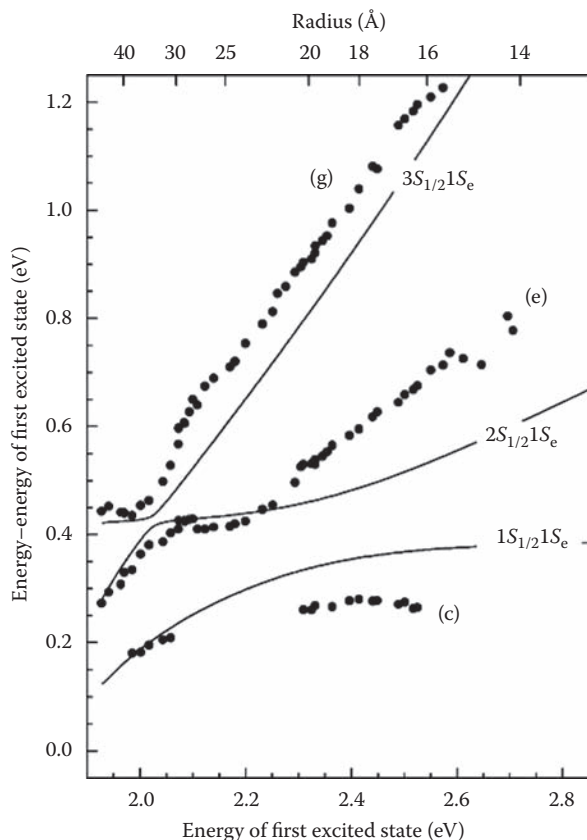
FIGURE 2.11 Theoretically predicted pair states (solid lines) assigned to features (c), (e), and (g) in Figure 2.7. The experimental data are shown for comparison (circles). (Adapted from Norris, D. J. and M. G. Bawendi, *Phys. Rev. B,* 53, 16338, 1996.)

overlap between the electron and hole, in small dots this term is strongly enhanced due to the confinement of the carriers.[81–84] Therefore, the right side of Figure 2.13 represents the small nanocrystal limit where the exchange interaction dominates. In this case, the important quantum number is the total angular momentum, N (see Figure 2.9). Because $F_h = 3/2$ and $F_e = 1/2$, the band-edge exciton is split into a fivefold degenerate $N = 2$ state and a threefold degenerate $N = 1$ state. In the middle of Figure 2.13, the correlation diagram between these two limits is shown. When both effects are included, the good quantum number is the projection of N along the unique crystal axis, N_m. The five sublevels are then labeled by $|N_m|$: one sublevel with $|N_m| = 2$, two with $|N_m| = 1$, and two with $|N_m| = 0$. Levels with $|N_m| > 0$ are twofold degenerate.

To include these effects into the theory, the anisotropy and exchange terms can be added as perturbations to the spherical model.[10] Figure 2.14 shows the calculated size dependence of the exciton fine structure. The five sublevels are labeled by $|N_m|$ with
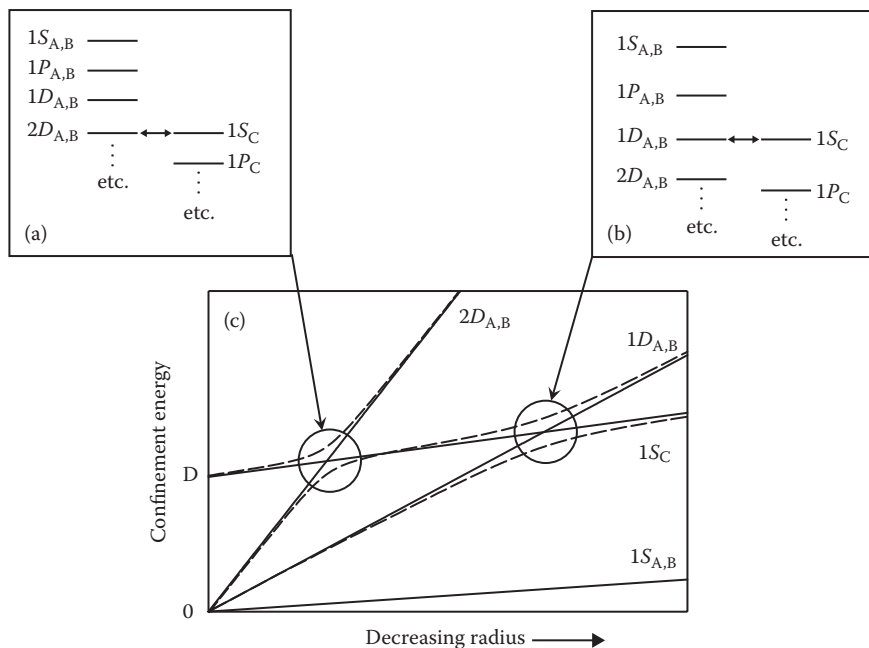
FIGURE 2.12 Cartoons depicting the origin of the observed avoided crossings. For a particular nanocrystal size, a resonance occurs between a hole level from the A and B bands (combined for simplicity) and a hole level from the C band. Energy-level diagrams for the hole states are shown in (a) and (b) for the two resonances responsible for the observed avoided crossings. (c) The energy of the hole states versus decreasing radius. The solid (dashed) lines represent the levels without (with) the valence band and *S-D* mixing.

superscripts to distinguish upper (U) and lower (L) sublevels with the same $|N_m|$. Their energy, relative to the 1^L sublevel, is plotted versus *effective radius*, which is defined as

$$a_{eff} = \frac{1}{2}\left(b^2 c\right)^{1/3} \tag{2.24}$$

where b and c are the short and long axes of the nanocrystal, respectively. The enhancement of the exchange interaction with decreasing nanocrystal size is clearly evident in Figure 2.14. Conversely, with increasing nanocrystal size the sublevels converge upon the bulk A-B splitting, as expected.

2.3.5 THE DARK EXCITON

At first glance, one may feel that the exciton fine structure is only a small refinement to the theoretical model with no real impact on the properties of nanocrystals. However, these splittings have helped explain a long-standing question in the emission behavior of CdSe nanocrystals. While exciton recombination in bulk II-VI semiconductors occurs with a ~1 ns lifetime,[86] CdSe quantum dots can exhibit
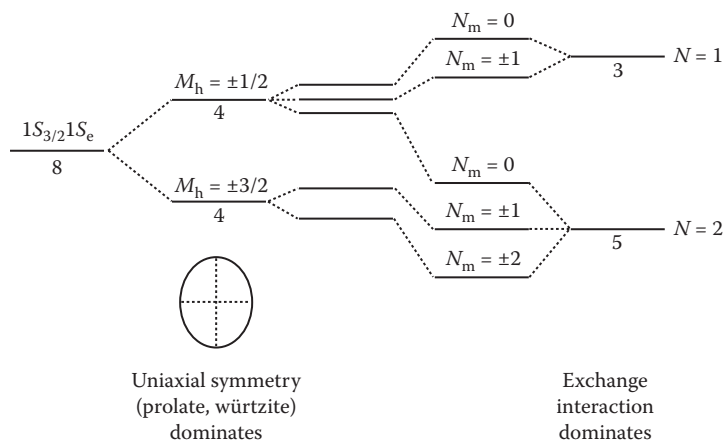
FIGURE 2.13 Energy-level diagram describing the exciton fine structure. In the spherical model, the band-edge exciton ($1S_{3/2}1S_e$) is eightfold degenerate. This degeneracy is split by the nonspherical shape of the dots, their hexagonal (wurtzite) lattice, and the exchange interaction.
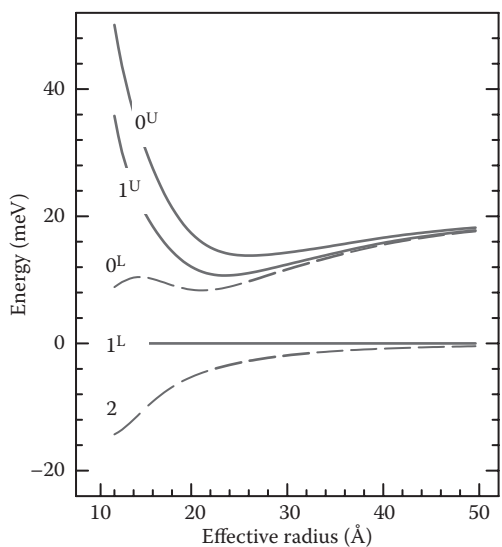

FIGURE 2.14 Calculated band-edge exciton structure versus effective radius. The sublevels are labeled by $|N_m|$ with superscripts to distinguish upper (U) and lower (L) sublevels with the same $|N_m|$. Positions are relative to 1^L. Optically active (passive) levels are shown as solid (dashed) lines. (Adapted from Norris, D. J., Al. L. Efros, M. Rosen, and M. G. Bawendi, *Phys. Rev. B,* 53, 16347, 1996.)

a ~1 μs radiative lifetime at 10 K.[10,87–90] This effect could perhaps be rationalized in early samples, which were of poor quality and emitted weakly via deep trap fluorescence. However, even high-quality samples, which emit strongly at the band edge, have long radiative lifetimes. To explain this behavior, the emission had been rationalized by many researchers as a *surface effect*. In this picture, the anomalous lifetime was explained by localization of the photoexcited electron or hole at the dot/matrix interface. Once the carriers are localized in surface traps, the decrease in carrier overlap increases the recombination time. The influence of the surface on emission was considered reasonable since these materials have such large surface-to-volume ratios (e.g., in a ~1.5 nm radius nanocrystal roughly one-third of the atoms are on the surface). This surface model could then explain the long radiative lifetimes, luminescence polarization results, and even the unexpectedly high LO phonon coupling observed in emission.

However, as first proposed by Calcott et al.,[81] the presence of exciton fine structure provides an alternative explanation for the anomalous emission behavior. Emission from the lowest band-edge state, $|N_m| = 2$, is optically forbidden in the electric dipole approximation. Relaxation of the electron–hole pair into this state, referred to as the *dark exciton*, can explain the long radiative lifetimes observed in CdSe QDs. Because two units of angular momentum are required to return to the ground state from the $|N_m| = 2$ sublevel, this transition is one-photon forbidden. However, less efficient, phonon-assisted transitions can occur, explaining the stronger LO-phonon coupling of the emitting state. In addition, polarization effects observed in luminescence[89] can be rationalized by relaxation from the 1^L sublevel to the dark exciton.[84]

2.3.6 Evidence for the Exciton Fine Structure

As mentioned earlier, PLE spectra from high-quality samples often exhibit additional structure within the lowest electron–hole pair state. For example, in Figure 2.4b, a narrow feature (α), its phonon replica (α′), and a broader feature (β) are observed. While these data alone are not sufficient to prove the origin of these features, a careful analysis of a larger data set has shown that they arise due to the exciton fine structure.[11] The analysis concludes that the spectra in Figure 2.4b are consistent with the absorption and emission lineshapes shown in Figure 2.15. In this case, the emitting state is assigned to the dark exciton ($|N_m| = 2$), the narrow absorption feature (α) is assigned to the 1^L sublevel, and the broader feature (β) is assigned to a combination of the 1^U and the 0^U sublevels. Since it is optically passive, the 0^L sublevel remains unassigned.

This assignment is strongly supported by size-dependent studies. Figure 2.16 shows PLE and FLN data for a larger sample (~4.4 nm effective radius). In Figure 2.4b three band-edge states are resolved: a narrow emitting state, a narrow absorbing state (α), and a broad absorbing state (β); whereas in Figure 2.16 four band-edge states are present: a narrow emitting state and three narrow absorbing states (α, $β_1$ and $β_2$). Consequently, $β_1$ and $β_2$ can be assigned to the individual 1^U and 0^U sublevels. To be more quantitative, a whole series of sizes can be examined (see Figure 2.17) to extract the experimental positions of the band-edge absorption and emission features as a function of size. In Figure 2.18b, the positions of the absorbing (filled circles and squares) and emitting (open circles) features are plotted relative to the narrow absorption line,
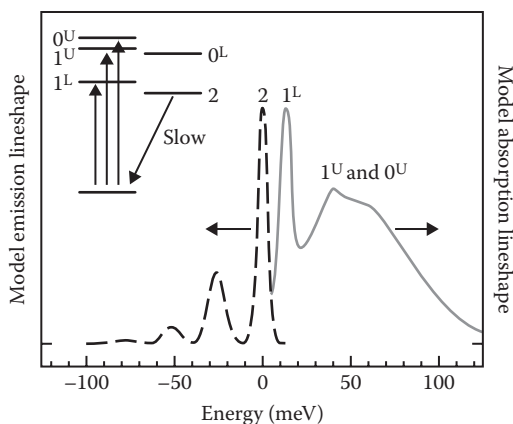
FIGURE 2.15 Absorption (solid line) and emission (dashed line) lineshape extracted for the sample shown in Figure 2.4 including LO-phonon coupling. An energy-level diagram illustrates the band-edge exciton structure. The sublevels are labeled as in Figure 2.14. Optically active (passive) levels are shown as solid (dashed) lines. (Adapted from Norris, D. J., Al. L. Efros, M. Rosen, and M. G. Bawendi, *Phys. Rev. B,* 53, 16347, 1996.)
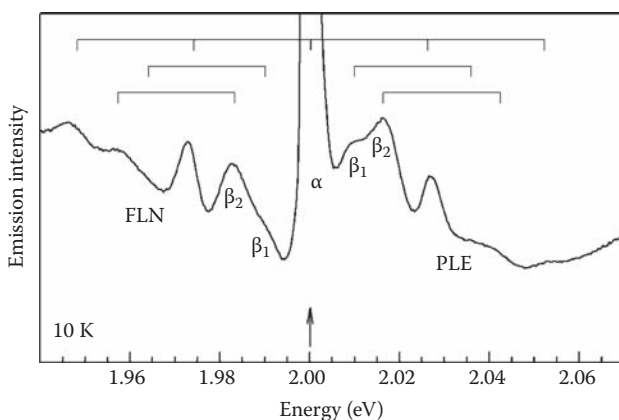

FIGURE 2.16 Normalized FLN and PLE data for a ~4.4 nm effective radius sample. The FLN excitation and PLE emission energies are the same and are designated by the arrow. Although emission arises from a single emitting state and its LO-phonon replicas, three over-lapping LO-phonon progressions are observed in FLN due to the three band-edge absorption features (α, β_1 and β_2). Horizontal brackets connect the FLN and PLE and features with their LO-phonon replicas. (Adapted from Norris, D. J., Al. L. Efros, M. Rosen, and M. G. Bawendi, *Phys. Rev. B,* 53, 16347, 1996.)

α (1^L). For larger samples, both the positions of β_1 and β_2 (pluses) and their weighted average (squares) are shown. Figure 2.18 shows the size dependence of the relative oscillator strengths of the optically allowed transitions. The strength of the upper states (1^U and 0^U) is combined since these states are not individually resolved in all of the data. Comparison of all of these data with theory (Figures 2.18a and c) indicates that
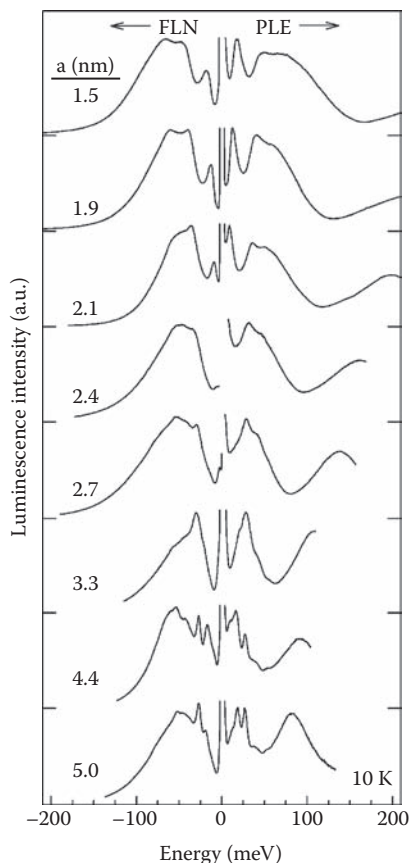
FIGURE 2.17 The size dependence of band-edge FLN/PLE spectra. (Adapted from Norris, D. J., Al. L. Efros, M. Rosen, and M. G. Bawendi, *Phys. Rev. B,* 53, 16347, 1996.)

the model accurately reproduces many aspects of the data. Both the splitting between $|N_m| = 2$ and 1^L (the Stokes shift) and the splitting between 1^L and the upper states (1^U and 0^U) are described reasonably well. Also, the predicted trend in the oscillator strength is observed. These agreements are particularly significant since, although the predicted structure strongly depends on the theoretical input parameters,[10] only literature values were used in the theoretical calculation.

2.3.7 EVIDENCE FOR THE "DARK EXCITON"

In addition to the observation that CdSe nanocrystals exhibit long emission lifetimes, they also display other emission dynamics that point to the existence of the dark exciton. For example, Figure 2.19a shows how the emission decay of a CdSe sample with a mean radius of 1.2 nm changes with an externally applied magnetic field. Obviously, the data indicate that the presence of a field strongly
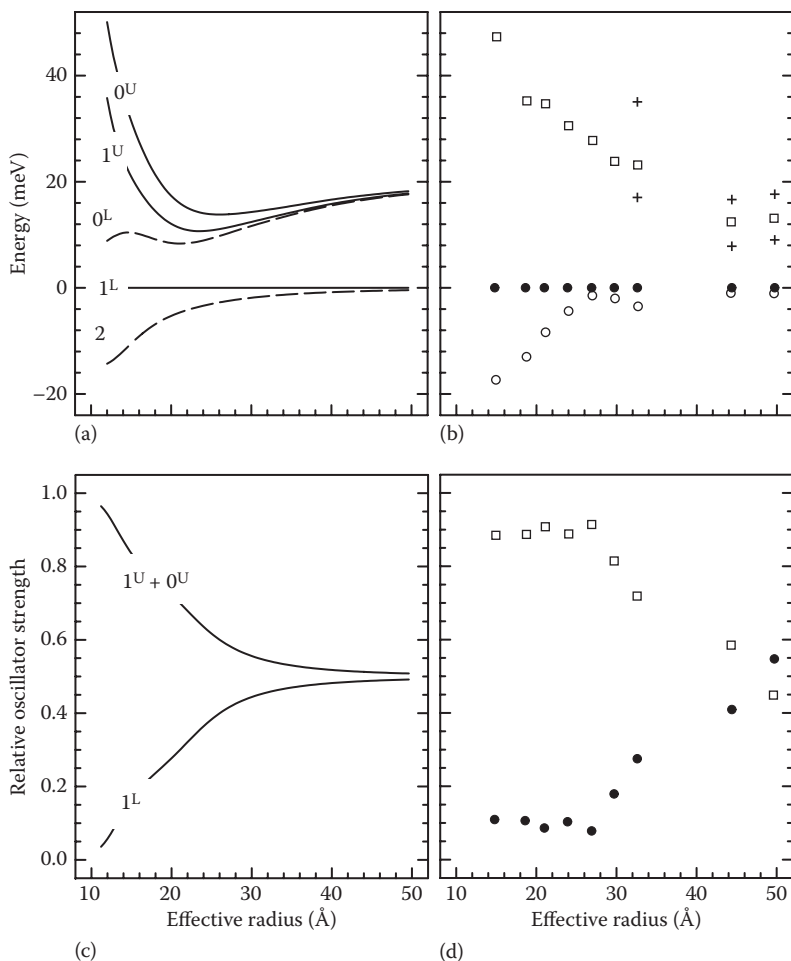
FIGURE 2.18 (a) Calculated band-edge exciton ($1S_{3/2}1S_e$) structure versus effective radius as in Figure 2.14. (b) Position of the absorbing (filled circles and squares) and emitting (open circles) features extracted from Figure 2.17. In samples where β_1 and β_2 are resolved, each position (shown as pluses) and their weighted average (squares) are shown. (c) Calculated relative oscillator strength of the optically allowed band-edge sublevels versus effective radius. The combined strength of 1^U and 0^U is shown. (d) Observed relative oscillator strength of the band-edge sublevels: 1^L (filled circles) and the combined strength of 1^U and 0^U (squares). (Adapted from Norris, D. J., Al. L. Efros, M. Rosen, and M. G. Bawendi, *Phys. Rev. B,* 53, 16347, 1996.)

modifies the emission behavior. This fact, which is difficult to explain with other models (e.g., due to surface trapping), is easily explained by the dark exciton model. Since thermalization processes are highly efficient, excited nanocrystals quickly relax into their lowest sublevel (the dark exciton). Furthermore, the separation between the dark exciton and the first optically allowed sublevel (1^L) is much larger than kT at cryogenic temperatures. Thus, the excited nanocrystal must return
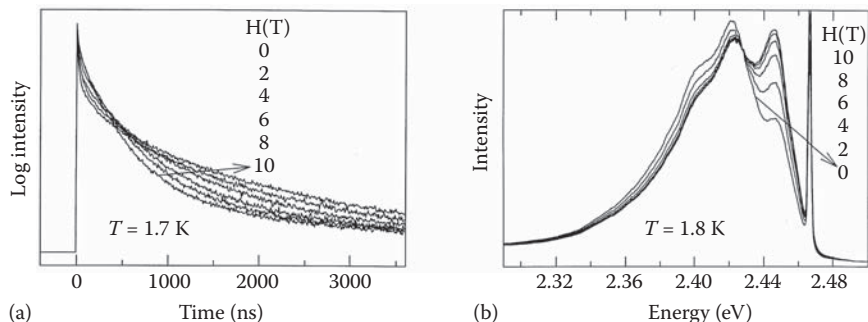
FIGURE 2.19 Magnetic field dependence of (a) emission decays recorded at the peak of the luminescence and (b) FLN spectra excited at the band edge (2.467 eV) for 1.2 nm radius CdSe nanocrystals. The FLN spectra are normalized to their one phonon line. A small amount of the excitation laser is included to mark the pump position. Experiments were carried out in the Faraday geometry (magnetic field parallel to the light propagation vector). (Adapted from Nirmal, M., D. J. Norris, M. Kuno, M. G. Bawendi, Al. L. Efros, and M. Rosen, *Phys. Rev. Lett.,* 75, 3728, 1995.)

to the ground state from the dark exciton. The long (μs) emission is consistent with recombination from this weakly emitting state. However, because a strong magnetic field couples the dark exciton to the optically allowed sublevels, the emission lifetime should decrease in the presence of a magnetic field. As the experimental fluorescence quantum yield remains essentially constant with field, this mixing leads to the decrease in the emission decay with increasing magnetic field.[10]

Another peculiar effect that can easily be explained by the dark exciton is the influence of a magnetic field on the vibrational spectrum, which is demonstrated in Figure 2.19b. A dramatic increase is observed in the relative strength of the zero-phonon-line with increasing field. This behavior results from the dark exciton utilizing the phonons to relax to the ground state. In a simplistic picture, the dark exciton would have an infinite fluorescence lifetime in zero applied field because the photon cannot carry an angular momentum of 2. However, nature will always find some relaxation pathway, no matter how inefficient. In particular, the dark exciton can recombine via a LO-phonon-assisted, momentum-conserving transition.[81] In this case, the higher phonon replicas are enhanced relative to the zero phonon line. If an external magnetic field is applied, the dark exciton becomes partially allowed due to mixing with the optically allowed sublevels. Consequently, relaxation no longer relies on a phonon-assisted process and the strength of the zero phonon line increases.

2.4 BEYOND CdSe

2.4.1 INDIUM ARSENIDE NANOCRYSTALS AND THE PIDGEON–BROWN MODEL

Success in both the synthesis and the spectroscopy of CdSe has encouraged researchers to investigate other semiconductor systems. Although the synthetic methods used

for CdSe can easily be extended to many of the II-VI semiconductors,[7,58] much effort has been focused on developing new classes of semiconductor nanocrystals, particularly those that may have high technological impact (e.g., silicon.[91,92]) Among these, the system that is perhaps best to discuss here is InAs. As a zinc blende, direct band gap, III-V semiconductor, InAs is in many ways very similar to CdSe. Most importantly, InAs nanocrystals can be synthesized through a well-controlled organometallic route that can produce a series of different-sized colloidal samples.[12] These samples exhibit strong band-edge luminescence such that they are well suited to spectroscopic studies. However, InAs also has several important differences from CdSe. In particular, it has a narrow band gap (0.41 eV). This implies that the coupling between the conduction and valence bands, which was largely ignored in our theoretical treatment of CdSe, will be important.

To explore this issue, Banin et al.[13,93,94] have performed detailed spectroscopic studies of high-quality InAs nanocrystals. Figure 6 in Chapter 8 shows size-dependent PLE data obtained from these samples. As in CdSe, the positions of all of the optical transitions can be extracted and plotted. The result is shown in Figure 7 in Chapter 8. However, unlike CdSe, InAs nanocrystals are not well described by a 6-band Luttinger Hamiltonian. Rather, the data requires an 8-band Kane treatment (also called the Pidgeon–Brown model,[37]) which explicitly includes coupling between the conduction and valence band.[13,41] With the 8-band model, the size dependence of the electronic structure can be well described, as shown in Figure 7 in Chapter 8.

Intuitively, one expects mixing between the conduction and valence band to become significant as the band gap decreases. Quantitatively, this mixing has been shown to be related to the expression

$$\sqrt{\frac{\Delta E_{e,h}}{E_g^s + \Delta E_{e,h}}} \tag{2.25}$$

where $\Delta E_{e,h}$ is the confinement energy of the electron or the hole.[41] As expected, the value of Equation 2.25 becomes significant as ΔE approaches the width of the band gap (i.e., in narrow band gap materials). However, unexpectedly, this equation also predicts that mixing can be significant in wide gap semiconductors due to the square root dependence. Furthermore, since the electron is typically more strongly confined than the hole, the mixing should be more important for the electrons. Therefore, this analysis concludes that even in wide gap semiconductors, an 8-band Pidgeon–Brown model may be necessary to accurately predict the size-dependent structure.

2.4.2 The Problem Swept under the Rug

Although the effective mass models can quite successfully reproduce many aspects of the electronic structure, the reader may be troubled by a problem that was "swept under the rug" in Section 2.3.3. In the discussion of the size-dependent data shown in Figure 2.7, it was mentioned that the data was plotted relative to the energy of the first excited state, in part to avoid a difficulty with the theory. This difficulty is shown more clearly in Figure 2.20, where the energy of the first excited state ($1S_{3/2}1S_e$) is plotted versus $1/a^2$. Surprisingly, the same theory that can quantitatively fit the data in Figures 2.10 and 2.11 fails to predict the size dependence of the lowest transition
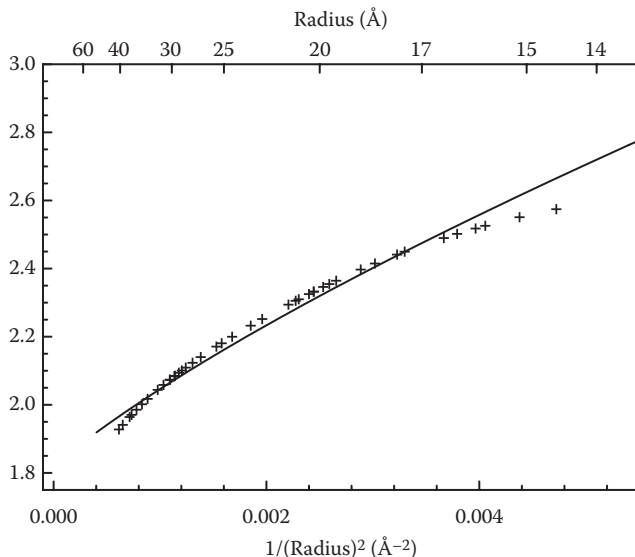
FIGURE 2.20 Energy of the first excited state ($1S_{3/2}1S_e$) in CdSe nanocrystals versus 1/radius[2]. The curve obtained from the same theory as in Figures 2.10 and 2.11 (solid line) is compared with PLE data (crosses). (Adapted from Norris, D. J. and M. G. Bawendi, *Phys. Rev. B,* 53, 16338, 1996.)

(Figure 2.20). Since the same problem arises in InAs nanocrystals (see Figure 7 in Chapter 8), where a more sophisticated 8-band effective mass model was used, it is unlikely that this is caused by the inadequacies of the 6-band Luttinger Hamiltonian. Rather, the experiment suggests that an additional nonparabolicity is present in the bands, which is not accounted for even by the 8-band model. However, the question remains: what is the cause of this nonparabolicity?

The observation that the theory correctly predicts the transition energies when plotted relative to the first excited state is an important clue. Since most of the low-lying optical transitions share the same electron level ($1S_e$), Figure 2.20 implies that the theory is struggling to predict the size dependence of the strongly confined electrons. By plotting relative to the energy of the first excited state, Figures 2.10 and 2.11 remove this troubling portion.[8] Then, the theory can accurately predict the transitions relative to this energy.

Since the underlying cause cannot be the mixing between the conduction and valence band, we must look for other explanations. Although the exact origin is still unknown, it is easy to speculate about several leading candidates. First, a general problem exists in how to theoretically treat the nanocrystal interface. In the simple particle-in-a-sphere model (Equation 2.2), the potential barrier at the surface was treated as infinitely high. This is theoretically desirable since it implies that the carrier wavefunction goes to zero at the interface. Of course, in reality, the barrier is finite and some penetration of the electron and hole into the surrounding medium must occur. This effect should be more dramatic for the electron, which is more strongly confined.

To partially account for this effect, the models used to treat CdSe and InAs nano-crystals incorporated a finite "square well" potential barrier, V_e, for the electron. (The hole barrier was still assumed to be infinite.) However, in practice, V_e became simply a fitting parameter to better correct for deviations in Figure 2.20. In addition, the use of a square potential barrier is not a rigorous treatment of the interface. In fact, how one should analytically approach such an interface is still an open theoretical problem. The resolution of this issue for the nanocrystal may require more sophisticated *general boundary condition* theories that have recently been developed.[95]

A second candidate to explain Figure 2.20 is the simplistic treatment of the Coulomb interaction, which is included only as a first-order perturbation. This approach not only misses additional couplings between levels, but also, as recently pointed out by Efros and Rosen,[41] ignores the expected size dependence in the dielectric constant. The effective dielectric constant of the nanocrystal should decrease with decreasing size. This implies that the perturbative approach underestimates the Coulomb inter-action. Unfortunately, this effect has not yet been treated theoretically.

Finally, one could also worry, in general, about the breakdown of the effective mass and the envelope function approximations in extremely small nanocrystals. As discussed in Section 2.2.2, nanocrystals that are much larger than the lattice constant of the semiconductor are required. In extremely small nanocrystals, where the diameter may only be a few lattice constants, this is no longer the case. Therefore, how small one can push the effective mass model before it breaks becomes an issue.

2.4.3 THE FUTURE

Clearly from the discussion in the last section, important problems remain to be solved before a complete theoretical understanding about the electronic structure in nanocrystals is obtained. However, hopefully this chapter has also demonstrated that we are clearly on the correct path. Further, theoretical issues are not the only area that needs attention. More experimental data are also necessary. Although much work has been done, it is surprising that after nearly two decades of work on high-quality nanocrystal samples, detailed spectroscopic studies have only been performed on two compound semiconductors, CdSe and InAs. Hopefully, in the coming years, this list will be expanded. For our understanding will be truly tested only by applying it to new materials.

ACKNOWLEDGMENTS

REFERENCES

1. Pankove, J. I., 1971. *Optical Processes in Semiconductors.* Dover, New York, p. 34.
2. Efros, Al. L. and Efros, A. L. (1982) *Sov. Phys. Semicond.* 16, 772.
3. Ekimov, A. I. and Onushchenko, A. A. (1982) *JETP Lett.* 34, 345.
4. Brus, L. E. (1983) *J. Chem. Phys.* 79, 5566.

5. Ekimov, A. I., Efros, Al. L. and Onushchenko, A. A. (1985) *Solid State Commun.* 56, 921.
6. Brus, L. E. (1984) *J. Chem. Phys.* 80, 4403.
7. Murray, C. B., Norris, D. J. and Bawendi, M. G. (1993) *J. Am. Chem. Soc.* 115, 8706.
8. Norris, D. J., Sacra, A., Murray, C. B. and Bawendi, M. G. (1994) *Phys. Rev. Lett.* 72, 2612.
9. Norris, D. J. and Bawendi, M. G. (1996) *Phys. Rev. B* 53, 16338.
10. Nirmal, M., Norris, D. J., Kuno, M., Bawendi, M. G., Efros, Al. L. and Rosen, M. (1995) *Phys. Rev. Lett.* 75, 3728.
11. Norris, D. J., Efros, Al. L., Rosen, M. and Bawendi, M. G. (1996) *Phys. Rev. B* 53, 16347.
12. Guzelian, A. A., Banin, U., Kadavanich, A. V., Peng, X. and Alivisatos, A. P. (1996) *Appl. Phys. Lett.* 69, 1432.
13. Banin, U., Lee, C. J., Guzelian, A. A., Kadavanich, A. V., Alivisatos, A. P., Jaskolski, W., Bryant, G. W., Efros, Al. L. and Rosen, M. (1998) *J. Chem. Phys.* 109, 2306.
14. Brus, L. (1991) *Appl. Phys. A* 53, 465.
15. Bányai, L. and Koch, S. W., 1993. *Semiconductor Quantum Dots*. World Scientific, Singapore.
16. Alivisatos, A. P. (1996) *J. Phys. Chem.* 100, 13226.
17. Alivisatos, A. P. (1996) *Science* 271, 933.
18. Woggon, U., 1997. *Optical Properties of Semiconductor Quantum Dots*. Springer-Verlag, Heidelberg.
19. Nirmal, M. and Brus, L. E. (1999) *Acc. Chem. Res.* 32, 407.
20. Gaponenko, S. V., 1999. *Optical Properties of Semiconductor Nanocrystals*. Cambridge University Press, Cambridge.
21. Eychmüller, A. (2000) *J. Phys. Chem. B* 104, 6514.
22. Ashcroft, N. W. and Mermin, N. D., 1976. *Solid State Physics*. Saunders, W.B., Orlando, FL.
23. Flügge, S., 1971. *Practical Quantum Mechanics,* Vol. 1. Springer, Berlin, p. 155.
24. Bastard, G., 1988. *Wave Mechanics Applied to Semiconductor Heterostructures*. Wiley, New York.
25. Altarelli, M., 1993. in *Semiconductor Superlattices and Interfaces*. A. Stella (Ed.), North Holland, Amsterdam, p. 217.
26. Xia, J. B. (1989) *Phys. Rev. B* 40, 8500.
27. Hellwege, K. H. (Ed.), 1982. in *Landolt-Bornstein Numerical Data and Functional Relationships in Science and Technology, New Series*. Springer-Verlag, Berlin, Vol. 17b, Group III.
28. Aven, M. and Prener, J. S., 1967. *Physics and Chemistry of II-VI Compounds*. North Holland, Amsterdam, p. 41.
29. Kittel, C., 1987. *Quantum Theory of Solids*. Wiley, New York.
30. Luttinger, J. M. (1956) *Phys. Rev. B* 102, 1030.
31. Luttinger, J. M. and Kohn, W. (1955) *Phys. Rev.* 97, 869.
32. Bir, G. L. and Pikus, G. E., 1974. *Symmetry and Strain-Induced Effects in Semiconductors*. Wiley, New York.
33. Lipari, N. O. and Baldereschi, A. (1973) *Phys. Rev. Lett.* 42, 1660.
34. Baldereschi, A. and Lipari, N. O. (1973) *Phys. Rev. B* 8, 2697.
35. Ge'lmont, B. L. and D'yakonov, M. I. (1972) *Sov. Phys. Semicond.* 5, 1905.
36. Kane, E. O. (1957) *J. Phys. Chem. Solids* 1, 249.
37. Pidgeon, C. R. and Brown, R. N. (1966) *Phys. Rev.* 146, 575.
38. Kane, E. O., 1980. in *Narrow Band Semiconductors. Physics and Applications, Lecture Notes in Physics*, W. Zawadzki (Ed.), Springer-Verlag, Berlin, Vol. 133.
39. Vahala, K. J. and Sercel, P. C. (1990) *Phys. Rev. Lett.* 65, 239.
40. Sercel, P. C. and Vahala, K. J. (1990) *Phys. Rev. B* 42, 3690.
41. Efros, Al. L. and Rosen, M. (1998) *Phys. Rev. B* 58, 7120.
42. Ekimov, A. I. and Onushchenko, A. A. (1984) *JETP Lett.* 40.

43. Rossetti, R., Hull, R., Gibson, J. M. and Brus, L. E. (1985) *J. Chem. Phys.* 82, 552.
44. Ekimov, A. I., Onushchenko, A. A. and Efros, Al. L. (1986) *JETP Lett.* 43, 376.
45. Chestnoy, N., Hull, R. and Brus, L. E. (1986) *J. Chem. Phys.* 85, 2237.
46. Borrelli, N. F., Hall, D. W., Holland, H. J. and Smith, D. W. (1987) *J. Appl. Phys.* 61, 5399.
47. Alivisatos, A. P., Harris, A. L., Levinos, N. J., Steigerwald, M. L. and Brus, L. E. (1988) *J. Chem. Phys.* 89, 4001.
48. Roussignol, P., Ricard, D., Flytzanis, C. and Neuroth, N. (1989) *Phys. Rev. Lett.* 62, 312.
49. Ekimov, A. I., Efros, Al. L., Ivanov, M. G., Onushchenko, A. A. and Shumilov, S. K. (1989) *Solid State Commun.* 69, 565.
50. Wang, Y. and Herron, N. (1990) *Phys. Rev. B* 42, 7253.
51. Müller, M. P. A., Lembke, U., Woggon, U. and Rückmann, I. (1992) *J. Noncryst. Solids* 144, 240.
52. Peyghambarian, N., Fluegel, B., Hulin, D., Migus, A., Joffre, M., Antonetti, A., Koch, S. W. and Lindberg, M. (1989) *IEEE J. Quantum Electron.* 25, 2516.
53. Esch, V., Fluegel, B., Khitrova, G., Gibbs, H. M., Jiajin, X., Kang, K., Koch, S. W., Liu, L. C., Risbud, S. H. and Peyghambarian, N. (1990) *Phys.Rev. B* 42, 7450.
54. Bawendi, M. G., Wilson, W. L., Rothberg, L., Carroll, P. J., Jedju, T. M., Steigerwald, M. L. and Brus, L. E. (1990) *Phys. Rev. Lett.* 65, 1623.
55. Ekimov, A. I., Hache, F., Schanne-Klein, M. C., Ricard, D., Flytzanis, C., Kudryavtsev, I. A., Yazeva, T. V., Rodina, A. V. and Efros, Al. L. (1993) *J. Opt. Soc. Am. B* 10, 100.
56. Bowen Katari, J. E., Colvin, V. L. and Alivisatos, A. P. (1994) *J. Phys. Chem.* 98, 4109.
57. Micic, O. I., Sprague, J. R., Curtis, C. J., Jones, K. M., Machol, J. L., Nozik, A. J., Giessen, H., Fluegel, B., Mohs, G. and Peyhambarian, N. (1995) *J. Phys. Chem.* 99, 7754.
58. Hines, M. A. and Guyot-Sionnest, P. (1998) *J. Phys. Chem. B* 102, 3655.
59. Norris, D. J., Yao, N., Charnock, F. T. and Kennedy, T. A. (2001) *Nano Lett.* 1, 3.
60. Peng, Z. A. and Peng, X. (2001) *J. Am. Chem. Soc.* 123, 168.
61. Hines, M. A. and Guyot-Sionnest, P. (1996) *J. Phys. Chem.* 100, 468.
62. Peng, X., Schlamp, M. C., Kadavanich, A. V. and Alivisatos, A. P. (1997) *J. Am. Chem. Soc.* 119, 7019.
63. Dabbousi, B. O., Rodriguez-Viejo, J., Mikulec, F. V., Heine, J. R., Mattoussi, H., Ober, R., Jensen, K. F. and Bawendi, M. G. (1997) *J. Phys. Chem. B* 101, 9463.
64. Moerner, W. E. and Orrit, M. (1999) *Science* 283, 1670.
65. Empedocles, S. A. and Bawendi, M. G. (1999) *Acc. Chem. Res.* 32, 389.
66. Hilinksi, E. F., Lucas, P. A. and Wang, Y. (1988) *J. Chem. Phys.* 89, 3435.
67. Park, S. H., Morgan, R. A., Hu, Y. Z., Lindberg, M., Koch, S. W. and Peyghambarian, N. (1990) *J. Opt. Soc. Am. B* 7, 2097.
68. Norris, D. J., Nirmal, M., Murray, C. B., Sacra, A. and Bawendi, M. G. (1993) *Z. Phys. D* 26, 355.
69. Gaponenko, S. V., Woggon, U., Saleh, M., Langbein, W., Uhrig, A., Müller, M. and Klingshirn, C. (1993) *J. Opt. Soc. Am. B* 10, 1947.
70. Woggon, U., Gaponenko, S., Langbein, W., Uhrig, A. and Klingshirn, C. (1993) *Phys. Rev. B* 47, 3684.
71. Kang, K. I., Kepner, A. D., Gaponenko, S. V., Koch, S. W., Hu, Y. Z. and Peyghambarian, N. (1993) *Phys. Rev. B* 48, 15449.
72. Kang, K., Kepner, A. D., Hu, Y. Z., Koch, S. W., Peyghambarian, N., Li, C.-Y., Takada, T., Kao, Y. and Mackenzie, J. D. (1994) *Appl. Phys. Lett.* 64, 1487–1489.
73. Norris, D. J. and Bawendi, M. G. (1995) *J. Chem. Phys.* 103, 5260.
74. Hoheisel, W., Colvin, V. L., Johnson, C. S. and Alivisatos, A. P. (1994) *J. Chem. Phys.* 101, 8455.
75. de Oliveira, C. R. M., Paula, A. M. d., Filho, F. O. P., Neto, J. A. M., Barbosa, L. C., Alves, O. L., Menezes, E. A., Rios, J. M. M., Fragnito, H. L., Cruz, C. H. B. and Cesar, C. L. (1995) *Appl. Phys. Lett.* 66, 439.

76. Rodriguez, P. A. M., Tamulaitis, G., Yu, P. Y. and Risbud, S. H. (1995) *Solid State Commun.* 94, 583.

77. Grigoryan, G. B., Kazaryan, E. M., Efros, A. L. and Yazeva, T. V. (1990) *Sov. Phys. Solid State* 32, 1031.

78. Koch, S. W., Hu, Y. Z., Fluegel, B. and Peyghambarian, N. (1992) *J. Cryst. Growth* 117, 592.

79. Efros, Al. L. (1992) *Phys. Rev. B* 46, 7448.

80. Efros, Al. L. and Rodina, A. V. (1993) *Phys. Rev. B* 47, 10005.

81. Calcott, P. D. J., Nash, K. J., Canham, L. T., Kane, M. J. and Brumhead, D. (1993) *J. Lumin.* 57, 257.

82. Takagahara, T. (1993) *Phys. Rev. B* 47, 4569.

83. Nomura, S., Segawa, Y. and Kobayashi, T. (1994) *Phys. Rev. B* 49, 13571.

84. Chamarro, M., Gourdon, C., Lavallard, P. and Ekimov, A. I. (1995) *Jpn. J. Appl. Phys.* 34-1, 12.

85. Kochereshko, V. P., Mikhailov, G. V. and Ural'tsev, I. N. (1983) *Sov. Phys. Solid State* 25, 439.

86. Henry, C. H. and Nassau, K. (1970) *Phys. Rev. B* 1, 1628.

87. O'Neil, M., Marohn, J. and McLendon, G. (1990) *J. Phys. Chem.* 94, 4356.

88. Eychmüller, A., Hasselbarth, A., Katsikas, L. and Weller, H. (1991) *Ber. Bunsenges. Phys. Chem.* 95, 79.

89. Bawendi, M. G., Carroll, P. J., Wilson, W. L. and Brus, L. E. (1992) *J. Chem. Phys.* 96, 946.

90. Nirmal, M., Murray, C. B. and Bawendi, M. G. (1994) *Phys. Rev. B* 50, 2293.

91. Littau, K. A., Szajowski, P. J., Muller, A. J., Kortan, A. R. and Brus, L. E. (1993) *J. Phys. Chem.* 97, 1224.

92. Wilson, W. L., Szajowski, P. F. and Brus, L. E. (1983) *Science* 262, 1242.

93. Banin, U., Lee, J. C., Guzelian, A. A., Kadavanich, A. V. and Alivisatos, A. P. (1997) *Superlattices and Microstruct.* 22, 559.

94. Cao, Y.-W. and Banin, U. (2000) *J. Am. Chem. Soc.* 122, 9692.

95. Rodina, A. V., Alekseev, A. Y., Efros, Al. L., Rosen, M. and Meyer, B. K. (2002) *Phys. Rev. B* 65, 125302.